Heat Transfer Engineering
Publication details, including instructions for authors and subscription information:
http://www.tandfonline.com/loi/uhte20

A Numerical Study on Natural Convention Heat Transfer From a Horizontal Isothermal Cylinder Located Underneath an Adiabatic Ceiling

Mehdi Ashjaee [a], Sajjad Bigham [b] & Sajad Yazdani [c]
[a] School of Mechanical Engineering, University of Tehran, Tehran, Iran
[b] Department of Mechanical and Aerospace Engineering, University of Florida, Gainesville, Florida, USA
[c] School of Energy, Kermanshah University of Technology, Kermanshah, Iran
Accepted author version posted online: 14 Nov 2013.Published online: 23 Dec 2013.

To cite this article: Mehdi Ashjaee, Sajjad Bigham & Sajad Yazdani (2014) A Numerical Study on Natural Convention Heat Transfer From a Horizontal Isothermal Cylinder Located Underneath an Adiabatic Ceiling, Heat Transfer Engineering, 35:10, 953-962, DOI: 10.1080/01457632.2014.859878

To link to this article: http://dx.doi.org/10.1080/01457632.2014.859878

Heat Transfer Engineering, 35(10):953–962, 2014

ISSN: 0145-7632 print / 1521-0537 online
DOI: 10.1080/01457632.2014.859878

A Numerical Study on Natural Convention Heat Transfer From a Horizontal Isothermal Cylinder Located Underneath an Adiabatic Ceiling

MEHDI ASHJAEE,[1] SAJJAD BIGHAM,[2] and SAJAD YAZDANI[3]

[1]School of Mechanical Engineering, University of Tehran, Tehran, Iran
[2]Department of Mechanical and Aerospace Engineering, University of Florida, Gainesville, Florida, USA
[3]School of Energy, Kermanshah University of Technology, Kermanshah, Iran

A numerical analysis is performed for steady-state and two-dimensional natural convection heat transfer from a horizontal isothermal cylinder located underneath a horizontal adiabatic ceiling. The finite-volume method based on the SIMPLE algorithm and a nonorthogonal grid discretization scheme are used to solve the continuity, momentum, and energy equations for the Rayleigh numbers in the range from 10^{-1} to 10^{4}. The Poisson equations are solved to find the grid points, which are distributed in a nonuniform manner with higher concentration close to the solid regions. In addition, the HYBRID differencing scheme is used for the approximation of the convective terms in the curvilinear coordinate. The effects of the Rayleigh numbers and cylinder spacing from the adiabatic ceiling on both the local and average Nusselt numbers around the cylinder are investigated. Numerical results are performed for the plate-to-cylinder spacing ranging from 0.1 to 1.4.

INTRODUCTION

Free convection heat transfer from a horizontal isothermal cylinder located underneath an adiabatic surface has various industrial applications. Typical examples are cylindrical resistors or capacitors underneath circuit boards, in which maximum or minimum heat transfer coefficient, as well as optimum spacing from the board, is important. Some industrial applications of this problem are cooling and casing design of electronic equipment, nuclear reactor safety, heat extraction from solar thermal storage devices, heating/ventilation/air conditioning (HVAC) industries, and the pipes carrying hot fluid that are often situated underneath an adiabatic surface.

Free convection heat transfer from a horizontal cylinder in a quiescent and infinite flow fluid has been extensively investigated analytically, numerically and experimentally [1–5]. Studies on free convection around a horizontal cylinder using interferometry and holography have been performed by [6, 7].

The effect of adiabatic confining walls on the heat transfer coefficient from a circular cylinder has been discussed by several researchers [8–14]. Sparrow and Ansari [15] investigated all modes of heat transfer from a horizontal cylinder situated adjacent to adiabatic, partially enclosing walls. Their experiments were performed in air for the Rayleigh numbers ranging from 2×10^4 to 2×10^5, the cylinder-to-vertical wall situated to the side of the cylinder (S_h), and the cylinder-to-horizontal wall beneath the cylinder (S_V), ranging from 1/12 to 4/3. When the cylinder interacts with a single horizontal wall, Sparrow and Ansari found that, for all the investigated spacing $1/12 \leq S_V \leq 4/3$, $Q/Q^* < 1$, the results indicate degradation in the cylinder heat transfer. The quantity Q is the cylinder heat transfer rate in the presence of wall–cylinder interactions, while Q^* denotes the cylinder heat transfer rate in the absence of interactions. The effect of a relatively narrow aluminum covered Bakelite plate above a horizontal heated cylinder at Grashof numbers in the

Address correspondence to Sajad Yazdani, School of Energy, Kermanshah University of Technology, Kermanshah, 67178-63766, Iran. E-mail: syazdani85@gmail.com

range from 2.1×10^6 to 3.2×10^6 was investigated by Saito et al. [16]. They found that the average Nusselt number around the cylinder was about 11% lower than that of a single cylinder in an infinite medium when it was placed at a distance of L/D ≈ 0.12 below the ceiling.

The free convection heat transfer rate from a heated cylinder underneath a wide isothermal ceiling was examined by Lawrence et al. [17] by using air as working fluid. They utilized a Mach–Zehnder interferometer and a finite-element-based code to perform their experiments. It was found that for cylinder-to-ceiling spacing greater than about one diameter the ceiling has almost no influence on heat transfer. For very close cylinder-to-ceiling spacing, the average Nusselt number increased substantially because of conduction effects. However, for $10^3 \leq \mathrm{Ra} \leq 10^5$ and L/D > 0.25, the effect of the ceiling on the numerically predicted overall heat transfer rate was less than 10%.

Koizumi and Hosokawa [18] investigated a natural convection flow around a cylinder located below a wide isothermal or an adiabatic ceiling. They used flow visualization to delineate the flow regime. Experiments were performed in air for the Rayleigh number ranging from 4.8×10^4 to 1×10^7. Their results showed the existence of three types of flow patterns depending on the Rayleigh number, the distance between the ceiling and cylinder, and the temperature condition of the ceiling for a variety of flow situations. At the Rayleigh number of $\mathrm{Ra} = 6 \times 10^5$, a steady two-dimensional flow was found for all values of the plate-to-cylinder spacing (L/D). At moderate and high Rayleigh numbers, an unsteady three-dimensional flow was observed for some low values of the plate-to-cylinder spacing, and the plume was noticed to oscillate laterally at high values of L/D. Local heat transfer coefficients around the cylinder were presented for both types of ceilings at $\mathrm{Ra} = 1.3 \times 10^6$ and L/D = 0.05, 0.2. Correa et al. [19] used a finite-difference code to delineate free convection temperature field around an isothermal horizontal cylinder placed under an adiabatic ceiling. Their results demonstrated that the ceiling had no effect on heat transfer rate for L/D > 2. By reducing cylinder-to-ceiling spacing less than half of the cylinder diameter, heat transfer rate decreases by 30% in comparison with a horizontal cylinder in a quiescent and infinite medium. By using a perfect adiabatic ceiling, the local Nusselt number around cylinder is different from those obtained by Koizumi and Hosokawa [18] for small cylinder-to-ceiling spacing.

Ashjaee et al. [20] presented an experimental and numerical investigation on two-dimensional free convection heat transfer from an isothermal horizontal cylinder located above an adiabatic surface. A Mach–Zehnder interferometer was used for carrying out the experimental section and the finite-volume method was applied for numerical section. They found that by increasing the Rayleigh number from 1 to 250, the interaction ratio decreases from 24.8% to 10.4%, respectively. Also, for the Rayleigh numbers ranging from 250 to 15000, the maximum interaction ratio is 3.5% for Ra = 4000 and L/D = 1.1. In addition, their results showed that the bottom wall–cylinder interactions can be neglected for L/D ≥ 1.1. Ashjaee et al. [21] investigated free convection heat transfer from a horizontal cylinder beneath an adiabatic ceiling by using a Mach–Zehnder interferometer for the values of L/D = 0.1, 0.3, 0.5, 0.7, 1.0, 1.5, and 2.4, and the Rayleigh number in a range from 1000 to 40,000. Their experimental results indicated that the adiabatic ceiling has no influence on free convection heat transfer from the cylinder for L/D ≥ 1.5. But by reducing this ratio from 1.5 to 0.5, the average Nusselt number decreases considerably. For L/D < 0.5, the average Nusselt number increases again due to the vortex formation at the top of the cylinder.

The objective of the current study is to numerically investigate the local and average free convection heat transfer coefficients from a horizontal isothermal cylinder located below a wide adiabatic ceiling at different Rayleigh numbers and cylinder-to-plate spacing (L/D). To obtain the hydrodynamic and thermal characteristics of the fluid flow, a numerical code based on the finite-volume method and nonorthogonal grid discretization scheme is developed to solve the governing equations. Numerical results are performed for the ratio of cylinder spacing to its diameter ranging from 0.1 to 1.4. Although electronic equipment functions at low Rayleigh numbers (Ra $\leq$ 100), in the literature, there are not any data about the problem at Ra < 1000. The lack of these necessary results and an applied investigation to cover the working ranges of electronic equipments caused us to focus on low Rayleigh numbers.

GOVERNING EQUATION

A horizontal cylinder of circular cross section underneath an adiabatic ceiling is considered. Free convection heat transfer occurs between the cylinder surface kept at uniform temperature T_w and the surrounding undisturbed fluid reservoir assumed at uniform temperature T_∞. The flow field and heat transfer are considered to be steady and laminar. The fluid is assumed to be incompressible, with constant physical properties and negligible viscous dissipation. Flow is modeled as "Boussinesq incompressible" to take coupling between energy and momentum equations into account. The nondimensional governing equations including continuity, momentum, and energy in a general nonorthogonal curvilinear coordinate framework with (ξ, η) as the independent variables can be expressed as follows [22, 23]:

Continuity equation:

$$\frac{\partial U^C}{\partial \xi} + \frac{\partial V^C}{\partial \eta} = 0 \tag{1}$$

ξ-Momentum equation:

$$\begin{aligned} &\frac{\partial}{\partial \xi}(uU^C) + \frac{\partial}{\partial \eta}(uV^C) \\ &= \frac{\partial}{\partial \xi}\left(q_{11}\frac{\partial u}{\partial \xi}\right) + \frac{\partial}{\partial \eta}\left(q_{22}\frac{\partial u}{\partial \eta}\right) + \frac{\partial}{\partial \xi}\left(q_{12}\frac{\partial u}{\partial \eta}\right) \\ &\quad + \frac{\partial}{\partial \eta}\left(q_{12}\frac{\partial u}{\partial \xi}\right) - \frac{\partial}{\partial \xi}(y_\eta p) + \frac{\partial}{\partial \eta}(y_\xi p) \end{aligned} \tag{2}$$

η-Momentum equation:

$$\frac{\partial}{\partial\xi}(vU^C)+\frac{\partial}{\partial\eta}(vV^C) = \frac{\partial}{\partial\xi}\left(q_{11}\frac{\partial v}{\partial\xi}\right)+\frac{\partial}{\partial\eta}\left(q_{22}\frac{\partial v}{\partial\eta}\right)+\frac{\partial}{\partial\xi}\left(q_{12}\frac{\partial v}{\partial\eta}\right) + \frac{\partial}{\partial\eta}\left(q_{12}\frac{\partial v}{\partial\xi}\right)+\frac{\partial}{\partial\xi}(x_\eta p)-\frac{\partial}{\partial\eta}(x_\xi p)+J.Gr.\theta \quad (3)$$

The energy equation is

$$\frac{\partial}{\partial\xi}(U^C\theta)+\frac{\partial}{\partial\eta}(V^C\theta) = \frac{\partial}{\partial\xi}\left[\left(\frac{q_{11}}{\mathrm{Pr}}\right)\frac{\partial\theta}{\partial\xi}\right]+\frac{\partial}{\partial\eta}\left[\left(\frac{q_{22}}{\mathrm{Pr}}\right)\frac{\partial\theta}{\partial\eta}\right] + \frac{\partial}{\partial\xi}\left[\left(\frac{q_{12}}{\mathrm{Pr}}\right)\frac{\partial\theta}{\partial\eta}\right]+\frac{\partial}{\partial\eta}\left[\left(\frac{q_{12}}{\mathrm{Pr}}\right)\frac{\partial\theta}{\partial\xi}\right] \quad (4)$$

where

$$U^C = uy_\eta - vx_\eta,\ V^C = -uy_\xi + vx_\xi,\ J = x_\xi y_\eta - x_\eta y_\xi,$$

$$q_{11} = \frac{1}{J}\left(y_\eta^2 + x_\eta^2\right),\ q_{12} = \frac{-1}{J}(x_\xi x_\eta + y_\xi y_\eta),$$

$$q_{11} = \frac{1}{J}\left(x_\xi^2 + y_\xi^2\right) \quad (5)$$

and the employed dimensionless variables are defined as follows:

$$x = \frac{x^*}{D},\ y = \frac{y^*}{D},\ u = \frac{u^*D}{v},\ v = \frac{v^*D}{v},\ p = \frac{p^*D^2}{\rho v^2},$$

$$\mathrm{Pr} = \frac{\nu}{\alpha},\ \theta = \frac{T-T_\infty}{T_W-T_\infty},\ Gr = \frac{g\beta(T_W-T_\infty)D^2}{\nu^2} \quad (6)$$

where u and v are the fluid velocity, p is the pressure, and T and T_∞ are the fluid temperature and the undisturbed surrounding fluid temperature, respectively.

To solve the problem, the nonorthogonal grid system is used to solve the mentioned equations. The grid points are generated by solving the Poisson equations for the physical domain and are distributed in a nonuniform manner with higher concentration close to the lines of AB and AD, as shown in Figure 1. Since the flow is symmetric about the vertical plane passing through the axes of the cylinder and adiabatic ceiling, the two-dimensional (2D) integration domain is assumed to extend from the vertical symmetry line and the half-cylinder surface up to a rectangular pseudo-boundary line set sufficiently far away from the cylinder.

Moreover, the appropriate boundary conditions have to be specified at each of the boundary lines that enclose the two-dimensional integration domain defined in the preceding.

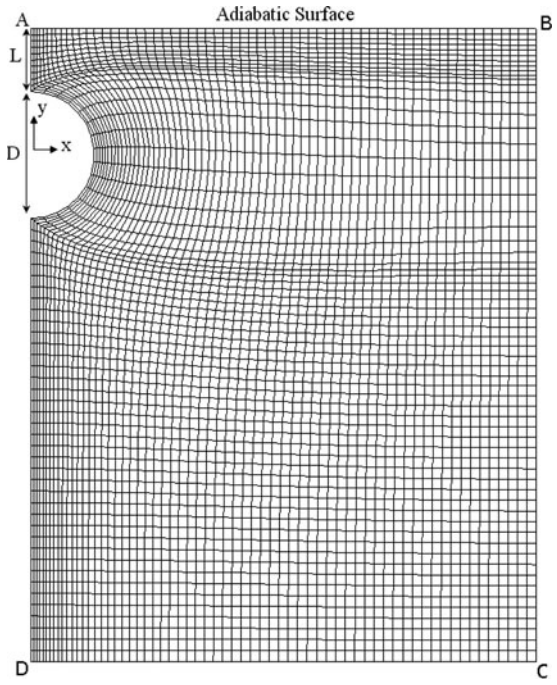

Figure 1 A schematic of the geometry, coordinate systems and grid generation.

The following boundary conditions are applied:

(a) The line AD is the left symmetry line, and therefore

$$u = \frac{\partial v}{\partial x} = \frac{\partial\theta}{\partial x} = 0 \quad (7)$$

(b) At the half-cylinder surface, the constant temperature boundary condition is applied:

$$\theta_w = 1\ u_w = v_w = 0 \quad (8)$$

(c) At the upper boundary condition (the line AB) the adiabatic boundary condition is applied:

$$\frac{\partial\theta}{\partial y} = 0\ u = v = 0 \quad (9)$$

(d) In the line BC, hydrodynamically and thermally fully developed boundary conditions are applied:

$$\frac{\partial u}{\partial x} = \frac{\partial v}{\partial x} = 0$$

$$u \geq 0 \text{ if} \frac{\partial\theta}{\partial x} = 0 \quad \text{or} \quad u < 0 \text{ if } \theta = 0 \quad (10)$$

(e) Again at the line CD, fully developed boundary condition is applied:

$$\frac{\partial u}{\partial y} = \frac{\partial v}{\partial y} = 0$$

$$v < 0 \text{ if } \frac{\partial\theta}{\partial y} = 0 \quad \text{or} \quad v \geq 0 \text{ if } \theta = 0 \quad (11)$$

SOLUTION PROCEDURES

The finite-volume method (FVM) based on the SIMPLE algorithm [24] is applied to solve the coupled nonlinear elliptic transport equations for u, v, p, and T in a "fully staggered" grid. In this type of grid, scalar variables such as the pressure and temperature at ordinary points are evaluated but the velocity components are calculated around the cell faces. Also, three different control volumes for u, v, and the scalar variables are used. A tri-diagonal matrix algorithm (TDMA) scheme is used to solve the discrete algebraic equations. In addition, the HYBRID differencing scheme [25] is used for approximation of the convective terms. The governing equations are solved by a successive overrelaxation method, and an underrelaxation technique is employed for convergence. One convergence criterion is a mass flux residual less than 10^{-8} for each control volume. Another criterion is $(|\varphi_{i+1} - \varphi_i|)/|\varphi_{i+1}| < 10^{-10}$ where φ represents any dependent variable, namely, u, v, and T, and i is the number of the iteration.

GRID DEPENDENCY

To ensure that the results of the numerical study are independent of the computational grid and the extent of the integration domain, two sensitivity analyses are carried out, namely, the grid sensitivity analysis and the integration domain size sensitivity analysis.

Generally, the accuracy of the solution and the time required for the solution are dependent on mesh refinement. In this work, the optimum grid is searched to have the appropriate run-time and enough accuracy. For instance, for the case of Ra = 100 and L/D = 0.2, three mesh sizes, 550 × 850, 600 × 900, and 650 × 950, are chosen and their effects on numerical results are studied. As shown in Figure 2a, for Ra = 100 and L/D = 0.2, a 600 × 900 grid seems to be optimum in accuracy and run time. Grid dependence studies have been completed with similar results for each numerical solution presented in the results section. However, throughout this study the results are only presented for the optimum grid.

Another investigation is performed to study the integration domain extent effect on the numerical results. For instance, for the case of Ra = 100 and L/D = 0.2, this study is depicted in Figure 2b. Three integration domain sizes, 6D × 6D, 8D × 8D, and 10D × 10D, are chosen and their effects on numerical results are studied. As shown, increasing the integration domain from 8D × 8D to 10D × 10D does not significantly change the local Nusselt number. Therefore, for this case, the 8D × 8D domain size for the integration domain is chosen. Furthermore, a similar type of integration domain extent study is carried out for the other Rayleigh numbers, not reported here, and the optimum domain size is chosen for each case.

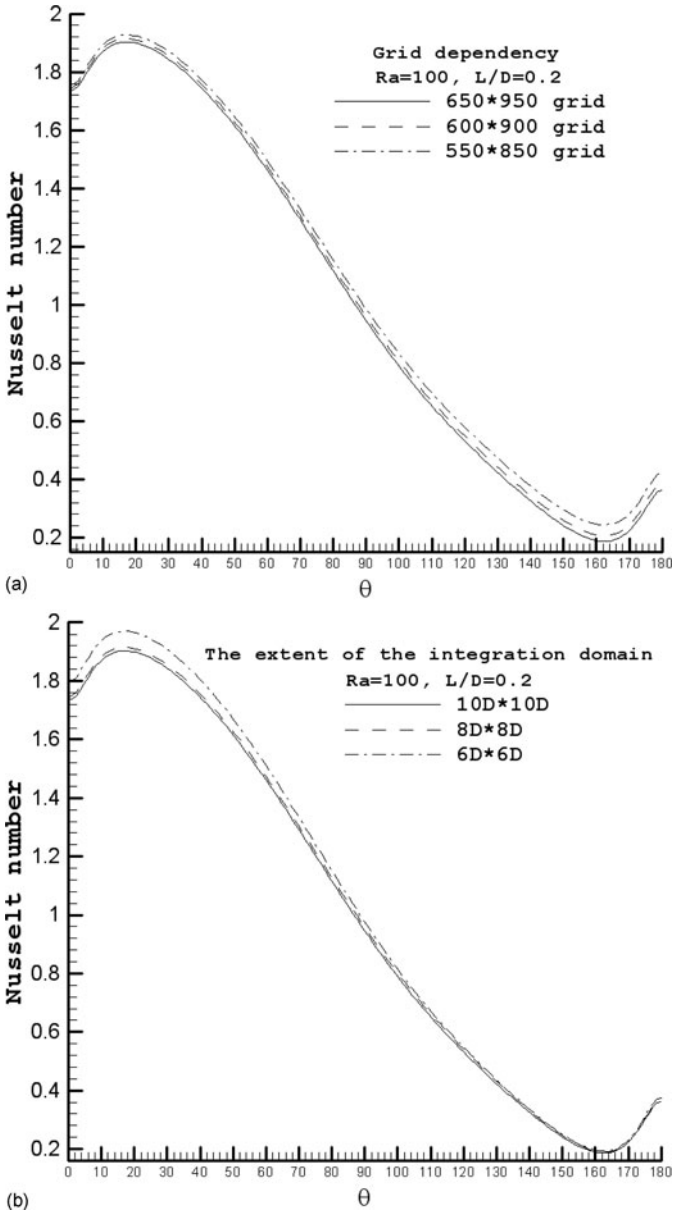

Figure 2 (a) Values of surface Nusselt numbers corresponding to three different computational grids. (b) Values of surface Nusselt numbers corresponding to three different integration domain extents.

VALIDATION

In order to validate the numerical code and nonorthogonal grid discretization scheme used in the present study, the average Nusselt numbers obtained at different Rayleigh numbers for a single cylinder set in free air are compared with the benchmark numerical data by Saitoh et al. [4], Cianfrini et al. [26], and other results available in the literature [1, 2, 4, 5, 27–30], as shown in Table 1, respectively. An excellent agreement between the present data and published results is noticed. As mentioned in the Introduction section, one of the closely related studies

Table 1 Comparison of the present results with experimental and numerical results and correlating equations found in the literatures

Ra	Present	[24]	[1]	[2]	[4]	[5]	[25]	[26]	[27]	[28]
10^1	1.415	1.421	1.31	1.057	—	1.4	1.49	1.49	—	—
10^2	1.891	1.961	2.02	1.599	—	2.05	2.1	2.11	—	2.07
10^3	3.166	3.023	3.11	2.563	3.024	3.09	3.14	3.14	3.06	3.04
10^4	4.804	4.819	4.8	4.278	4.826	4.94	4.97	4.92	4.86	4.85

belongs to Ashjaee et al. [21]. The numerical results of the current work and experimental results of reference [21] are validated for Ra = 10^4 and the plate-to-cylinder spacing ranging from 0.1 to 1.4 in Table 2. An overall good agreement between the present data and experimental results is noticed. The major difference between the numerical results of the present work and the experimental data returns to the uncertainty of the experimental data. The experimental data of reference [21] are obtained from the correlation that is presented in their paper with standard deviation of about ±4.7% and with maximum and minimum error of 9.31% and 2.61%, respectively.

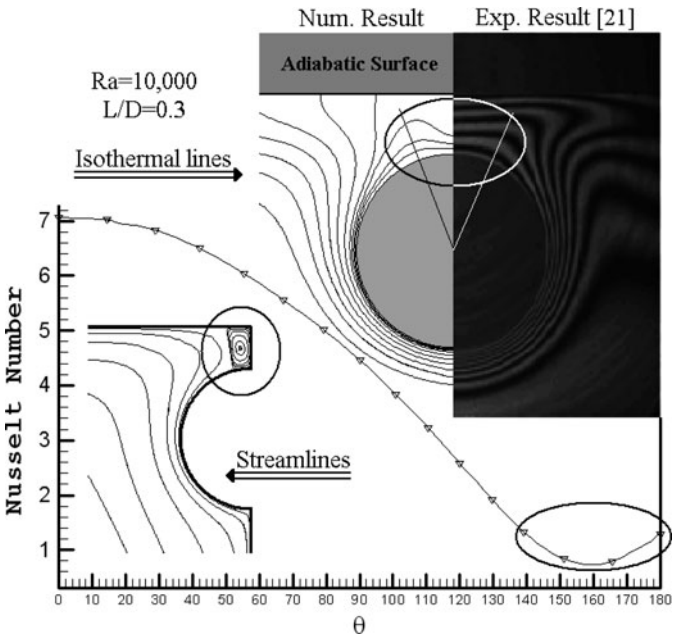

Figure 3 The isothermal lines, the streamlines, and the local heat transfer coefficient for the case of Ra = 10^4 and L/D = 0.3.

RESULTS AND DISCUSSION

Effects of the Rayleigh number and cylinder spacing from the adiabatic ceiling on the local and average Nusselt numbers around the cylinder are investigated. Numerical results are presented for the Rayleigh numbers ranging from 10^{-1} to 10^4. Because of the symmetrical geometry, in this work, only one half of domain is numerically solved. Therefore, the time of computation work reduces considerably. Also, the numerical simulations are performed for Pr = 0.71, which corresponds to the air.

It is favorable to describe the main phenomenological aspects of the problem. For this reason, for the case of Ra = 10^4 and L/D = 0.3, the isothermal lines, the streamlines, and the local heat transfer coefficient are depicted in Figure 3. At first, close to the bottom of the heated cylinder, fresh fluid is heated. The fluid is inclined to move upward when it is heated. Therefore, the fluid moves upward to form a thermal boundary layer at sufficiently high Rayleigh numbers. Afterward, as the air plume follows the cylinder surface, it keeps gaining heat and the thickness of the thermal boundary layer increases. Thus, the local heat transfer coefficient decreases. The presence of the ceiling causes the fluid velocity to decrease. In other words, the ceiling magnifies the decrease in the local heat transfer coefficient by decreasing the air plume velocity. An interesting phenomenon is observed in the cases of L/D = 0.1–0.3. In these cases, as shown in the streamlines, the formation of vortices at the top of the cylinder and their enhancement effect on heat transfer overcome the damping effects of the ceiling and the boundary-layer thickness on the heat transfer coefficient. Therefore, the local heat transfer coefficient increases.

Figure 4 illustrates the streamline contours close to the cylinder for Ra = 1000 and 10,000 and L/D ratios of 0.3 and 0.7. For Ra = 1000 and 10,000 at L/D = 0.3, Figures 4a and 4c indicate the formation of a vortex flow, which affects the local Nusselt number at the top of the cylinder. To see whether the flow remains truly steady and the pressure field does not cause the vortices to move around, some numerical experiments have been conducted by solving the governing equations for the whole domain rather than the vertical symmetry condition. The new runs indicate that the results did not noticeably change and the pressure field did not cause the vortices to move around or tend to interact with each other. On the other hand, for Ra = 1000 and 10,000 at L/D = 0.7, it can be seen from Figures 4b and 4d that there is not any vortex flow around the cylinder. This means that when the plate-to-cylinder spacing increases, the strength of the vortices decreases.

Table 2 Comparison of the present results with experimental results of reference [21]

L/D	0.1	0.2	0.3	0.5	0.7	0.9	1.1	1.4
Present	3.655173	3.873563	4.080696	4.287829	4.506219	4.676179	4.778179	4.7907
Reference [21]	4.1914	3.8232	3.7073	3.7898	4.0504	4.3209	4.531	4.7167

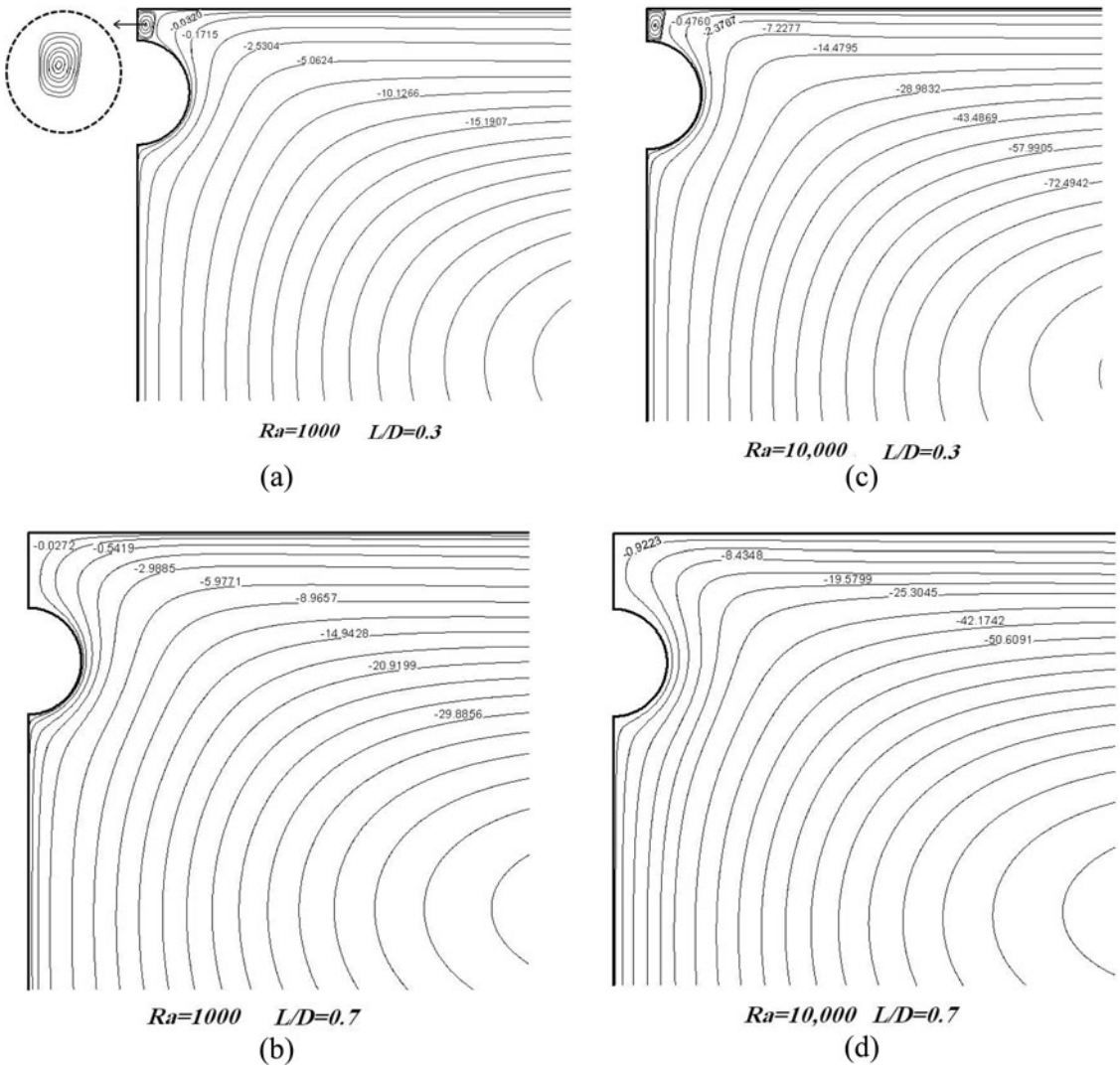

Figure 4 A diagram of the streamlines for (a) Ra = 1000, L/D = 0.3 (b) Ra = 1000, L/D = 0.7, (c) Ra = 10,000, L/D = 0.3, and (d) Ra = 10,000, L/D = 0.7.

Figures 5 and 6 display the isotherm lines around the cylinder for the Rayleigh numbers of 10^1 and 10^4, respectively. In all diagrams, the cylinder surface indicates the nondimensional temperature corresponding to unity. All of the diagrams indicate that the air plume from the heated cylinder will rise around the angle of $\theta = 180^\circ$ and hit the adiabatic ceiling. As the cylinder-to-ceiling spacing decreases, the air plume gets suppressed from rising vertically due to the damping effect of the ceiling. This causes the air plume to flow toward the left and right sides.

The variation of the local Nusselt numbers versus L/D is shown in Figure 7 for the Rayleigh numbers of Ra = 1, 10^2, and 10^4. It can be noticed that the local Nusselt number decreases as the value of θ increases. The physical reason is that by increasing the value of θ, the thickness of thermal boundary layer around the cylinder increases and consequently it intensifies the thermal resistant effect. Furthermore, these figures demonstrate that as the cylinder-to-ceiling spacing increases, the local Nusselt number increases for each Ra number at a specified angle. This increase in the Nusslet number is mainly due to a decrease in the ceiling damping effect.

For the case of Ra = 1, it is found that the damping effect of the ceiling is more sensible for $\theta \geq 110^\circ$. However, the ceiling damping effect can be seen for all angles as the Ra number increases. Also, as expected, at L/D = 1.1 and 1.4 the trend of the local Nusselt number becomes more similar to that of a horizontal isothermal cylinder in quiescent and infinite air. In addition, the figures illustrate an increase in the local Nusselt number for L/D = 0.1, 0.2, and 0.3 at approximately $\theta \geq 160^\circ$. This increase in the local heat transfer coefficient is due to the formation of the vortex flow at the top of the cylinder.

Figure 8 shows the variations of the average Nusselt numbers in terms of L/D and Rayleigh numbers. It can be seen that for each Ra number, as the plate-to-cylinder spacing increases, the average Nusselt number increases toward its value as the

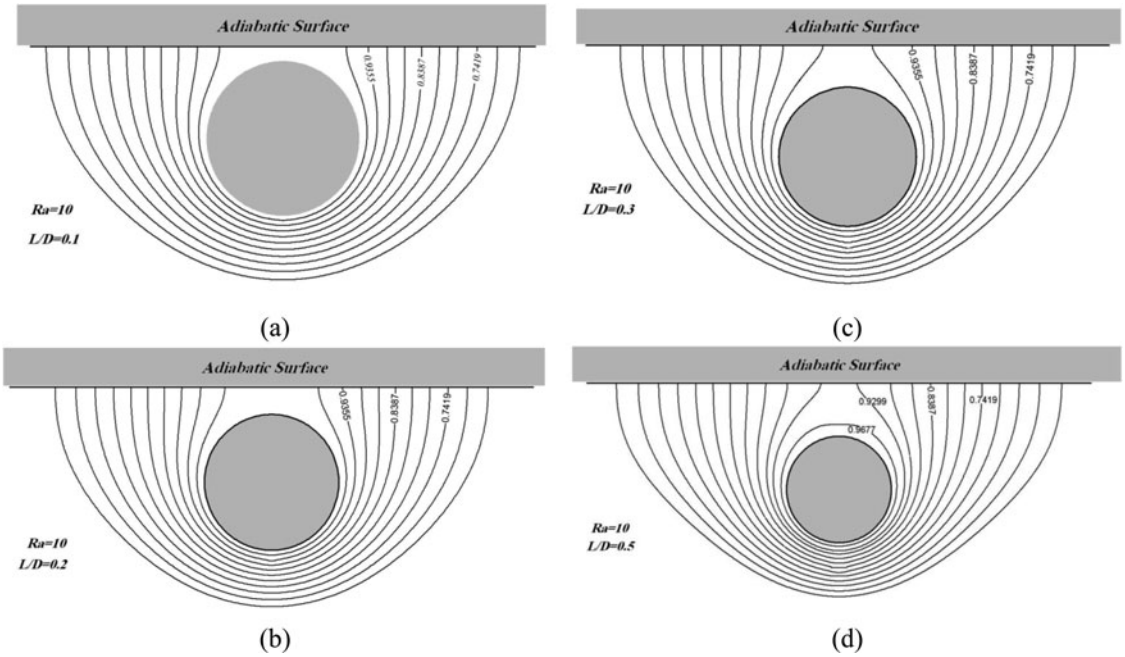

Figure 5 The isotherm lines around the cylinder for Ra = 10 and (a) L/D = 0.1, (b) L/D = 0.2, (c) L/D = 0.3, and (d) L/D = 0.5.

cylinder is in the free air. In fact, the effect of the upper surface on the flow and thermal patterns in the region between the top of the cylinder and the adiabatic surface decreases as the value of L/D increases. In addition, for any assigned geometry, the average Nusselt number increases with increasing the Rayleigh number, owing to the increase in buoyancy force.

As mentioned, for L/D = 0.1, 0.2 and 0.3, the formation of the vortex flow at the upper side of the cylinder, approximately at $\theta \geq 160^{\circ}$, caused an increase in the local Nusselt number. However, from Figure 8 it can be found that this vortex flow cannot considerably influence the overall amount of Nusselt number due to its low strength and narrow affected location.

For the case of Ra $\leq$ 10, Figure 8 also indicates that the average Nusselt number is less than unity. This means the main heat transfer mechanism occurs by conduction heat transfer. Therefore, the major part of the heat is transferred by the conductive heat transfer rather than the convective heat transfer.

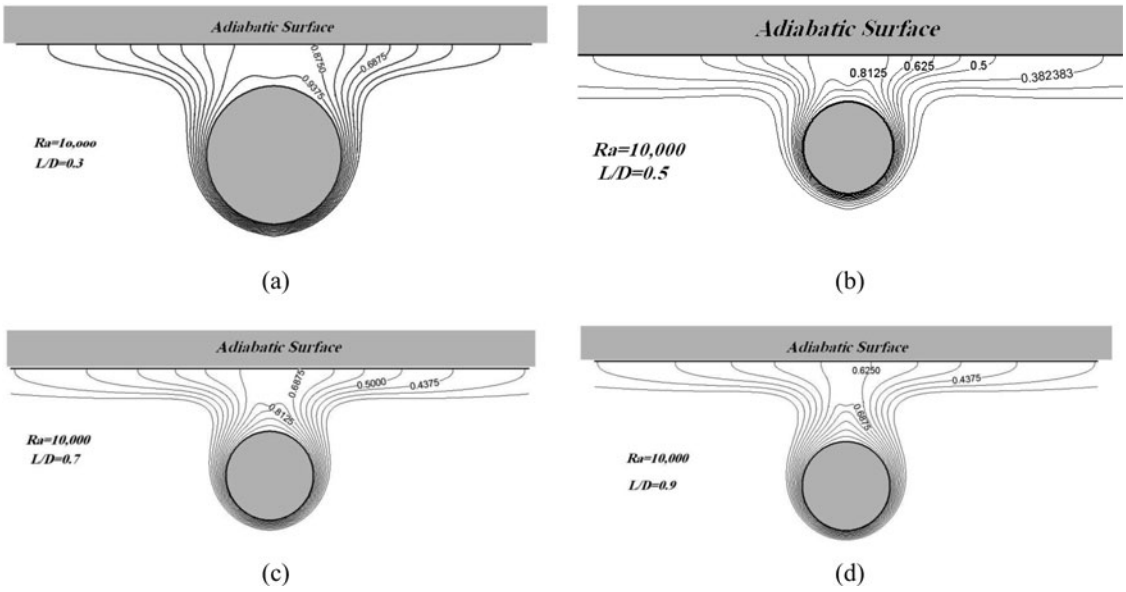

Figure 6 The isotherm lines around the cylinder for Ra = 10,000 and (a) L/D = 0.3, (b) L/D = 0.5, (c) L/D = 0.7, and (d) L/D = 0.9.

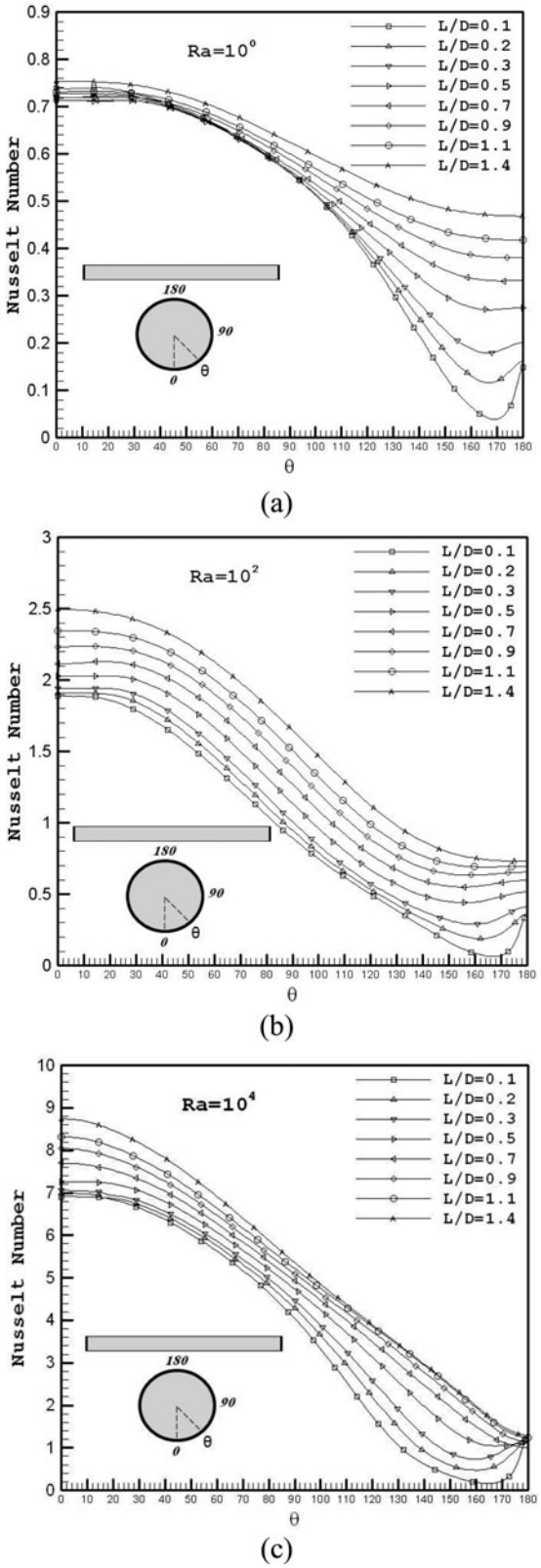

Figure 7 Local Nusselt numbers versus θ (a) Ra = 1, (b) Ra = 100, and (c) Ra = 10,000.

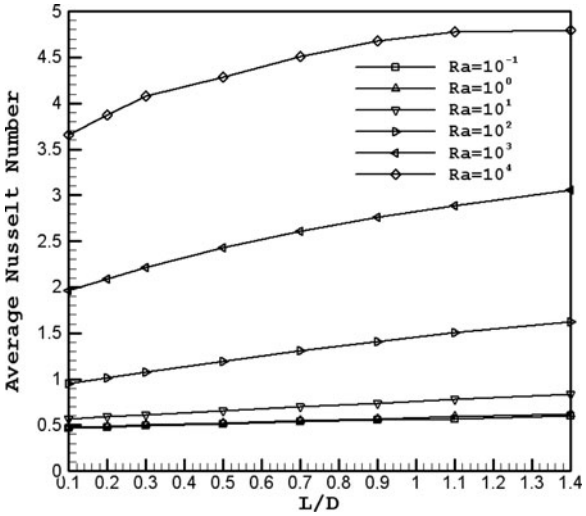

Figure 8 Average Nusselt numbers versus L/D.

Also, for Ra = 10,000, a comparison between the results of the current work in the case of L/D = 0.1 and reference [1] in the case of L/D = ∞ illustrates a maximum decrease of 24.4% in the average heat transfer coefficient. Furthermore, this comparison shows that the damping effect of the adiabatic ceiling can be neglected for the case of Ra = 10,000 and L/D = 1.4.

CONCLUSIONS

The effects of the aspect ratio and Rayleigh number on natural convection heat transfer from an isothermal horizontal cylinder located underneath an adiabatic ceiling have been numerically investigated. Governing equations including continuity, momentum, and energy are discretized using the finite-volume method and solved by the SIMPLE algorithm in nonorthogonal curvilinear coordinate framework at Rayleigh numbers ranging from 10^{-1} to 10^4. The main results obtained can be summarized as follows:

1. At each Ra number, the local heat transfer coefficient decreases by both increase in the value of θ and decrease in the cylinder-to-ceiling spacing.
2. For L/D = 0.1, 0.2, and 0.3 the numerical results indicate the formation of a vortex flow, which increases the local Nusselt number at the top of the cylinder.
3. For each Ra number, the average Nusselt number increases as the plate-to-cylinder spacing increases.
4. For each L/D, the average Nusselt number increases with increasing the Rayleigh number.
5. For Ra = 10,000, a maximum decrease of 24.4% in the average heat transfer coefficient from the cylinder under the adiabatic ceiling in the case of L/D = 0.1 is revealed in comparison with a single cylinder in the free air.

6. For Ra $\leq$ 10, the results show that the major part of the heat transfer occurred by the conductive heat transfer mechanism rather than by convective heat transfer.

NOMENCLATURE

D	cylinder diameter (m)
g	gravitational acceleration (m/s^2)
Gr	Grashof number ($\frac{g\beta(T_w-T_\infty)D^3}{\nu^2}$)
J	Jacobian of the coordinate transformation
k	thermal conductivity of air (W/m-K)
L	cylinder -to- adiabatic surface distance (m)
p	pressure (Pa)
Pr	Prandtl number (Pr $= \nu/\alpha$)
Q	cylinder heat transfer rate in the presence of wall–cylinder interactions
Q^*	cylinder heat transfer rate in the absence of wall–cylinder interactions
q_{11}	parameter defined in Eq. (5)
q_{12}	parameter defined in Eq. (5)
q_{22}	parameter defined in Eq. (5)
Ra	Rayleigh number ($g\beta\,(T_w - T_\infty)\,L^3/\alpha\nu$)
T	temperature (K)
U	velocity component in ξ direction (m/s)
u	dimensionless horizontal velocity component
V	velocity component in η direction (m/s)
v	dimensionless vertical velocity component
x	dimensionless horizontal coordinate
y	dimensionless vertical coordinate

Greek Symbols

α	thermal diffusivity (m^2/s)
β	volumetric expansion coefficient (1/K)
ρ	density of fluid (kg/m^3)
η	curvilinear vertical coordinate
θ	angle from stagnation point (degree)
ν	kinematic viscosity (m^2/s)
ξ	curvilinear horizontal coordinate

Subscripts

∞	ambient condition
w	cylinder surface

Superscripts

C	contravariant velocities
*	refers to dimensional parameters

REFERENCES

[1] Morgan, V. T., The Overall Convective Heat Transfer From Smooth Circular Cylinders, *Advances in Heat Transfer*, vol. 11, pp. 199–264, 1975.

[2] Churchill, S. W., and Chu, H. H. S., Correlating Equations for Laminar and Turbulent Free Convection From a Horizontal Cylinder, *International Journal of Heat and Mass Transfer*, vol. 18, pp. 1049–1053, 1975.

[3] Kitamura, K., Kami-iwa, F., and Misumi, T., Heat Transfer and Fluid Flow of Natural Convection Around Large Horizontal Cylinders, *International Journal of Heat and Mass Transfer*, vol. 42, pp. 4093–4106, 1999.

[4] Saitoh, T., Sajiki, T., and Maruhara, K., Bench Mark Solution to Natural Convection Heat Transfer Problem Around the Horizontal Circular Cylinder, *International Journal of Heat and Mass Transfer*, vol. 36, pp. 1251–1259, 1993.

[5] Kuehn, T. H., and Goldstein, R. J., Numerical Solution to the Navier–Stokes Equations for Laminar Natural Convection About a Horizontal Isothermal Circular Cylinder, *International Journal of Heat and Mass Transfer*, vol. 23, pp. 971–979, 1980.

[6] Herraez, J. V., and Belda, R., A Study of Free Convection in Air Around Horizontal Cylinders of Different Diameters Based on Holographic Interferometry: Temperature Field Equations and Heat Transfer Coefficients, *International Journal of Thermal Science*, vol. 41, pp. 261–267, 2002.

[7] Ambrosini, D., Paoletti, D., and Spagnolo, G. Schirripa, Study of Free-Convective Onset on a Horizontal Wire Using Speckle Pattern Interferometry, *International Journal of Heat and Mass Transfer*, vol. 46, pp. 4145–4155, 2003.

[8] Masters, G. F., Natural Convection Heat Transfer From a Horizontal Cylinder in the Presence of Nearby Walls, *Canadian Journal of Chemical Engineering*, vol. 53, pp. 144–149, 1975.

[9] Farouk, B., and Guceri, S., Natural and Mixed Convection Heat Transfer Around a Horizontal Cylinder Within Confining Walls, *Numerical Heat Transfer*, vol. 35, pp. 329–341, 1982.

[10] Sparrow, S., and Pfeil, D., Enhancement of Natural Convection Heat Transfer From a Horizontal Cylinder Due to Vertical Shrouding Surface, *ASME Journal of Heat Transfer*, vol. 106, pp. 124–130, 1984.

[11] Karim, F., Farouk, B., and Nnmer, L., Natural Convection Heat Transfer From a Horizontal Cylinder Between Vertical Confining Adiabatic Walls, *ASME Journal of Heat Transfer*, vol. 108, pp. 291–298, 1986.

[12] Sadeghipour, M. S., and Kazemzadeh, S. H., Transient Natural Convection From a Horizontal Cylinder Confined Between Vertical Walls: A Finite Element Solution, *International Journal of Numerical Methods in Engineering*, vol. 34, pp. 621–635, 1992.

[13] Ma, L., Vander Zaden, J., van der Kooi, J., and Nieuwestadt, F. T. M., Natural Convection Around a Horizontal

Circular Cylinder in Infinite Space and Within Confining Plates: A Finite Element Solution, *Journal of Numerical Heat Transfer, Part A*, vol. 25, pp. 441–456, 1994.

[14] Sadeghipour, M. S., and Razi, Y. P., Natural Convection From a Horizontal Cylinder: The Optimum Distance Between the Confining Walls, *International Journal of Heat and Mass Transfer*, vol. 44, pp. 367–374, 2001.

[15] Sparrow, E. M., and Ansari, M. A., All-Modes Heat Transfer From a Horizontal Cylinder Situated Adjacent to Adiabatic, Partially Enclosing Walls, *International Journal of Heat and Mass Transfer*, vol. 22, no. 10, pp. 1855–1864, 1984.

[16] Saito, T., Ishiguro, R., and Fujishima, Y., Natural Convection Heat Transfer Around a Horizontal Cylinder (Effect of a Horizontal Plate Placed Above the Cylinder), *Proceeding of the Sixth National Heat Transfer Symposium of Japan* (in Japanese), pp. 61–64, 1969.

[17] Lawrence, G. B., Jardine, G. E., Naylor, D., and Machin, A. D., Free Convection From a Horizontal Heated Cylinder Located Below a Ceiling, *Transaction of the CSME*, vol 23, pp. 19–35, 1998.

[18] Koizumi, H., and Hosokawa, I., Chaotic Behavior and Heat Transfer Performance of Natural Convection Around a Hot Horizontal Cylinder Affected by a Flat Ceiling, *International Journal of Heat and Mass Transfer*, vol. 39, pp. 1081–1091, 1996.

[19] Correa, M., Parra, R., Vidal, A., Rodriguez, J., Aguilera, M. E., and Gonzalez, D., Natural Convection Around a Horizontal Cylinder Near an Adiabatic Cover Wall, *Proceeding of Fourth ICCHMT*, pp. 336–339, May 17–20, 2005, Paris, France.

[20] Ashjaee, M., Yazdani, S., Bigham, S., and Yousefi, T., Experimental and Numerical Investigation on Free Convection from a Horizontal Cylinder Located Above an Adiabatic Surface, *Heat Transfer Engineering*, vol. 33, no. 3, pp. 213–224, 2012.

[21] Ashjaee, M., Eshtiaghi, A. H., Yaghoubi, M., and Yousefi, T., Experimental Investigation on Free Convection From a Horizontal Cylinder Beneath an Adiabatic Ceiling, *Journal of Experimental Thermal and Fluid Science*, vol. 32, pp. 614–623, 2007.

[22] Bigham, S., Shokouhmand, H., Isfahani, R. N., and Yazdani, S., Fluid Flow and Heat Transfer Simulation in a Constricted Microchannel: Effects of Rarefaction, Geometry, and Viscous Dissipation, *Numerical Heat Transfer, Part A*, vol. 59, pp. 209–230, 2011.

[23] Shokouhmand, H., Bigham, S., Slip-flow and Heat Transfer of Gaseous Flows in the Entrance of a Wavy Microchannel, *International Communications in Heat and Mass Transfer*, vol. 37, pp. 695–702, 2010.

[24] Patankar, S. V., *Numerical Heat Transfer and Fluid Flow*, McGraw-Hill, New York, NY, 1980.

[25] Spalding, D. B., A Novel Finite Difference Formulation for Differential Expressions Involving Both First and Second Derivatives, *International Journal of Numerical Methods Eng*, vol. 4, pp. 551–559, 1972.

[26] Cianfrini, C., Corcione, M., and Habib, E., Free Convection Heat Transfer From a Horizontal Cylinder Affected by a Downstream Parallel Cylinder of Different Diameter, *International Journal of Thermal Sciences*, vol. 45, pp. 923–931, 2006.

[27] Raithby, G. D., and Hollands, K. G. T., Laminar and Turbulent Free Convection From Elliptic Cylinders With a Vertical Plate and Horizontal Circular Cylinder as Special Cases, *Journal of Heat Transfer*, vol. 98, pp. 72–80, 1976.

[28] Kuehn, T. H., and Goldstein, R. J., Correlating Equations for Natural Convection Heat Transfer Between Horizontal Circular Cylinders, *International Journal of Heat and Mass Transfer*, vol. 19, pp. 1127–1134, 1976.

[29] Wang, P., Kahawita, R., and Nguyen, T. H., Numerical Computation of the Natural Convection Flow About a Horizontal Cylinder Using Splines, *Journal of Numerical Heat Transfer*, vol. 17, pp. 191–215, 1990.

[30] Clemes, S. B., Hollands, K. G. T., and Brunger, A. P., Natural Convection Heat Transfer From Long Horizontal Isothermal Cylinders, *Journal of Heat Transfer*, vol. 116, pp. 96–104, 1994.

Mehdi Ashjaee is a professor of thermal fluid science at University of Tehran, Tehran, Iran. He received his Ph.D. in 1986 from the University of Wisconsin–Madison. His main research interests are forced, free convection heat transfer problems using interferometry and holography, specifically in heat exchangers. He also has worked on spray fields with swirl injectors extensively using phase Doppler anemometry. He has published more than 50 articles in well-recognized journals and proceedings.

Sajjad Bigham is a Ph.D. candidate at the University of Florida. He received his M.Sc. degree from the University of Tehran, Iran, in 2009. His main research interests are heat transfer phenomena in microchannels, free and mixed convection heat transfer problems using interferometry and holography, nanofluids heat transfer, two-phase flow modeling, and computational fluid dynamics (CFD). He has cooperated in founding of the nanofluids heat transfer and laser diagnostic laboratories at Kermanshah University of Technology. He has published more than 15 articles in well-known journals and proceedings.

Sajad Yazdani is a faculty member of the Mechanical Engineering Department at Kermanshah University of Technology. He received his M.Sc. degree from the University of Tehran, Iran, in 2009. His main research interests are free and mixed convection heat transfer problems using interferometry and holography, nanofluids heat transfer, heat transfer in microchannels, two-phase flow phenomena, and CFD. He is founder and director of the nanofluids heat transfer and laser diagnostic laboratories at Kermanshah University of Technology. He has published more than 15 articles in well-known journals and proceedings.